Characterization of Glioma Microcirculation and Tissue Features Using Intravoxel Incoherent Motion Magnetic Resonance Imaging in a Rat Brain Model

Mami Iima, MD,† Olivier Reynaud, PhD,† Tomokazu Tsurugizawa, PhD,† Luisa Ciobanu, PhD,† Jing-Rebecca Li, PhD,†‡ Françoise Geffroy, B. Tech,† Boucif Djemai, B. Tech,† Masaki Umehana, BSc,§ and Denis Le Bihan, MD, PhD†||*

Purpose: Our aim was to investigate the pertinence of diffusion and perfusion magnetic resonance imaging (MRI) parameters obtained at 17.2 T in a 9L glioma rat brain tumor model to evaluate tumor tissue characteristics.

Materials and Methods: The local animal ethics advisory committee approved this study. 9L glioma cells were injected intracerebrally to 14 Fischer rats. The animals were imaged at 7 or 12 days after implantation on a 17.2-T MRI scanner, using 72 different b values (2–3025 s/mm^2). The signal attenuation, S/So, was fitted using a kurtosis diffusion model (ADCo and K) and a biexponential diffusion model (fractions f_{fast} and f_{slow} and diffusion coefficients D_{fast} and D_{slow}) using b values greater than 300 s/mm^2. To bridge the 2 models, an average diffusion coefficient $<D>$ and a biexponential index were estimated from the biexponential model as ADCo and K equivalents, respectively. Intravoxel incoherent motion perfusion–related parameters were obtained from the residual signal at low b values, after the diffusion component has been removed. Diffusion and perfusion maps were generated for each fitted parameter on a pixel-by-pixel basis, and regions of interest were drawn in the tumor and contralateral side to retrieve diffusion and perfusion parameters. All rats were killed and cellularity and vascularity were quantitatively assessed using histology for comparison with diffusion and perfusion parameters.

Results: Intravoxel incoherent motion maps clearly highlighted tumor areas as generally heterogeneous, as confirmed by histology. For diffusion parameters, ADCo and $<D>$ were not significantly different between the tumor and contralateral side, whereas K in the tumor was significantly higher than in contralateral basal ganglia ($P < 0.0001$), as well as biexponential index ($P < 0.001$). ADCo and $<D>$ in the tumor at day 7 were significantly higher than at day 12 ($P < 0.01$ and $P < 0.001$, respectively). f_{IVIM} in the tumor from the kurtosis diffusion model was significantly higher than in contralateral basal ganglia ($P < 0.001$). f_{IVIM} in the tumor at day 7 was significantly higher than in the tumor at day 12 ($P < 0.0001$). There was no significant difference for D* between the tumor and contralateral side ($P = 0.06$). A significant negative correlation was found between tumor vascularity and f_{IVIM} ($P < 0.05$) as well as between tumor cell count and $<D>$ ($P < 0.01$).

Conclusion: Quantitative non-Gaussian diffusion and perfusion MRI can provide valuable information on microvasculature and tissue structure to improve characterization of brain tumors.

Key Words: IVIM MRI, non-Gaussian diffusion, perfusion, glioma, brain

(*Invest Radiol* 2014;00: 00–00)

Received for publication October 26, 2013; and accepted for publication, after revision, December 31, 2013.

From the *Department of Diagnostic Imaging and Nuclear Medicine, Kyoto University Graduate School of Medicine, Kyoto, Japan; †NeuroSpin, CEA-Saclay, Gif-sur-Yvette, France; ‡Equipe DEFI, INRIA Saclay Palaiseau, France; §Kyoto University Faculty of Medicine; and ||Human Brain Research Center, Kyoto University Graduate School of Medicine, Kyoto, Japan.

Conflicts of interest and sources of funding: Support was received through a grand-in-aid for JSPS Fellows from the Japan Society for the Promotion of Science (no. 25-2430).

Reprints: Mami Iima, MD, Department of Diagnostic Imaging and Nuclear Medicine, Kyoto University Graduate School of Medicine, 54 Shogoin-kawaharacho, Sakyo-ku, Kyoto 606-8507, Japan. E-mail: mamiiima@kuhp.kyoto-u.ac.jp.

ISSN: 0020-9996/14/0000–0000

Gliomas, the most common primary tumors of the brain, vary histologically from low grade to high grade, and even a single tumor mass frequently shows considerable histological heterogeneity.[1] Diffusion magnetic resonance imaging (MRI) has appeared as a potential imaging biomarker for cancer diagnosis,[2] as it has been observed that the water apparent diffusion coefficient (ADC) measured in tumors decrease significantly in various tumors, including brain tumors.[3,4] Conversely, the ADC returns to normal under successful radiotherapy or chemotherapy, and some groups have suggested that diffusion MRI could be used to assess treatment efficacy or failure well before early clinical symptoms become visible.[5] The sensitivity of the ADC to cell density has been established,[5] and a putative mechanism for this drop in ADC could be the increase in the density of cell membranes (caused by cell proliferation) that act as obstacles for water diffusion.[6] Because of such membrane interactions, water diffusion in tissues is not free (Gaussian). Patterns of non-Gaussian diffusion, which are better observed when using strong diffusion encoding (high b values), require more advanced analysis models than the ADC does.[7] On the other hand, diffusion MRI is also sensitive to perfusion because the flow of blood water in randomly oriented capillaries mimics a diffusion process. This "pseudodiffusion" effect, known as "intravoxel incoherent motion" (IVIM),[8,9] has been proposed to evaluate perfusion in tissues.[10,11] This approach has increasingly been used to investigate brain and body cancer tissues for which vascularity is a key parameter, not only to characterize tumors but also to predict or monitor therapeutic responses or tumor recurrences.[11–13] The degree of neovasculization is critical in assessing tumor grade and malignancy and also in understanding tumor biology.[14] Although angiogenesis is an obligate feature of tumor growth and results in new microvessels in brain tumors, the molecular biology of this process is still unknown. A key feature of IVIM diffusion MRI is that it does not involve contrast agents, an alternative for perfusion MRI, as some agents are contraindicated in patients exposed to the risk of nephrogenic systemic fibrosis.[15]

In this study, we evaluated the behavior of the parameters of the IVIM perfusion model and of 2 non-Gaussian diffusion models, namely, the kurtosis[16] and the biexponential[17] models, in the rat brain after implantation of a 9L glioma tumor. Experiments were performed using a 17.2-T MRI scanner to reach high spatial resolution and estimate the diffusion and perfusion model parameters with a reasonable accuracy, which requires a high signal-to-noise ratio. Results were compared with histological findings regarding vessel and cell density.

MATERIALS AND METHODS

Animals and Implantation of Tumor Cells

All of the animal experiments were conducted according to recommendations of the EU Directive 2010/63/EU and the French National Committee (87/848) for care and use of laboratory animals. A total of 14 Fischer rats weighing 200 to 350 g were used for the experiments. They were housed with free access to food and water, on a 12:12-hour day/night cycle (lights on from 6:00 AM to 6:00 PM), with room temperature maintained at approximately 20°C.

9L rat glioma cells were cultivated in Dulbecco's modified Eagle's medium supplemented with 10% fetal bovine serum, 1% glutamine, 1% penicillin/streptomycin, and 3.5% glucose and 1% pyruvate. Cultures were incubated in a controlled atmosphere at 37°C with 5% CO_2 and passaged 2 or 3 times a week. The glioma cells (5 μL) were stereotactically implanted in the rats' caudate putamen. The rats were first anesthetized with a ketamine/domitor mixture and placed in a stereotactic frame. A 2-cm scalp incision was made on the left side of the skull, 3 mm left from the midline, 5 mm deep from the surface at the bregma level, to allow the passage of a Hamilton syringe to inject 5 μL 9L rat glioma cells. Rats were imaged 7 days (6 rats) or 12 days (8 rats) after implantation.

Magnetic Resonance Imaging

Data were acquired on a 17.2-T MRI scanner (Bruker Biospec, Billerica, MA) using an in-house ^{1}H transmit/receive surface coil of 3-cm diameter. For all magnetic resonance acquisitions, the rats were anesthetized with 1% to 3% isoflurane in an air/O_2 mix (50:50) and maintained still in the magnet using ear bars and a bite bar connected to the nose cone. The respiration rate was monitored and the body temperature was maintained at 37°C with a heated water pad throughout the MRI study.

Coronal T2-weighted (T2w) images were acquired using a rapid acquisition with relaxation enhancement sequence with the following parameters: repetition time, 3000 milliseconds; echo time, 15 milliseconds; in-plane resolution, 156 × 156 μm^2; matrix size, 128 × 128; field of view, 20 × 20 mm^2; slice thickness, 1 mm; total scan time, 3 minutes 12 seconds.

Coronal diffusion MRI images were acquired using a standard pulsed-gradient echo-planar imaging spin-echo sequence. A total of 72 *b* values (25 *b* values ranging from 2 to 160 s/mm^2, 35 *b* values ranging from 172.5 to 935 s/mm^2, and 12 *b* values ranging from 1150 to 3025 s/mm^2) were acquired. The acquisition parameters were set as follows: maximum gradient strength, 1 T/m; gradient direction, [$X = 1$, $Y = 1$, $Z = 1$]; diffusion time, 11.2 milliseconds (gradient pulse duration, 2.5 milliseconds; gradient pulse interval, 12 milliseconds); in-plane resolution, 312 × 312 μm^2; matrix size, 64 × 64; field of view 20 × 20 mm^2; slice thickness, 1 mm, 4 segments; repetition time, 3000 milliseconds; echo time, 21 milliseconds; 6 averages. The acquisition time for each *b* value was 72 seconds, for a total acquisition time of 86 minutes 24 seconds.

Histopathology and Immunohistochemistry

The rats were killed immediately after the MRI session for histological analysis. The rats were subjected to intravenous perfusion with physiological saline solution to remove circulating blood and with a 4% paraformaldehyde solution to fix the brain. The brains were harvested from the above animals and immersed successively in different solutions as follows: 2 hours at 4°C in a 4% paraformaldehyde solution for tissue fixation, 12 hours in 15% sucrose, and finally, 48 hours in 30% sucrose solution for cryoprotection. Brain tissues were sectioned using a cryostat (Microm HM 560, Thermo Scientific) to obtain 10-μm-thick slices encompassing a significant section of the tumor. The von Willebrand factor (vWF) was used to detect/count endothelial cells, and 4',6-diamidino-2-phenylindole staining was used to reveal cell nuclei. Finally, as a reference for visualizing the tumor, an adjacent slice was stained with hematoxylin and erythrosine (H&E) (Sigma-Aldrich, St Louis, MO).

For staining the endothelial cells, frozen tissues were sectioned (10 μm thick) and mounted on positively charged slides. Samples were washed 2 times with phosphate buffered saline (PBS), incubated with protein blocking solution containing 1% bovine serum albumin, 1.5% triton, and 5% normal goat serum in PBS for 2 hours at room temperature, and then incubated with the appropriate dilution of rabbit anti-mouse/rat/human vWF antibody (abcam, Cambridge, UK) for 1 hour at room temperature. After the samples were rinsed 2 times (5 minutes each) with PBS, the slides were incubated with the appropriate dilution of secondary Dylight conjugated goat antirabbit antibody (abcam) for 1 hour at room temperature, avoiding light exposure. Then, all the sections were washed with PBS 3 times (5 minutes each). Endothelial cells were identified by orange fluorescence for vWF. For H&E staining, 10-μm-thick cryostat sections of the brains were washed with PBS. The sections were stained with hematoxylin at room temperature for 1 minute, washed with lithium carbonate solution for 1 minute and with water for several seconds, and then stained with eosin for 1 minute. After washing, the sections were air dried, mounted, coverslipped, and viewed under a light microscope. General tissue morphology and mitotic figures were visualized by H&E staining.

Data Processing

Intravoxel incoherent motion parameters were obtained from the signal attenuation, S/So, in 2 steps, first estimating the diffusion component, F_{diff}, using the kurtosis or biexponential diffusion model, then estimating the perfusion component, F_{perf}, from the residual signal, after the diffusion component has been removed:

$$\text{S/So} = f_{\text{IVIM}} F_{\text{perf}} + (1 - f_{\text{IVIM}}) F_{\text{diff}} , \quad (1)$$

where f_{IVIM} is the (T1w, T2w) volume fraction of incoherently flowing blood in the tissue. This 2-step process was motivated to increase robustness (as there are fewer parameters to estimate for each step) and justified because IVIM perfusion effects are not expected to contribute to the signal for *b* values above 300 s/mm^2. (The cutoff value for the IVIM effects was determined after examination of a few cases: after the removal of the diffusion component, the residual signal was found not to differ significantly from noise for *b* values above 300 s/mm^2). Hence, the signal attenuation, $[(1 - f_{\text{IVIM}})F_{\text{diff}}]$, for *b* greater than 300 s/mm^2 was first fitted using a kurtosis model equation:

$$F_{\text{diff}} \approx \exp\left[-b\text{ADCo} + (b\text{ADCo})^2 \, K/6 \right] , \quad (2)$$

where *b* is the degree of diffusion sensitization of the MRI sequence and ADCo is the virtual ADC (derivative of F_{diff}), which could be obtained when *b* approaches 0. The dimensionless coefficient *K* (kurtosis) characterizes the degree of deviation of the signal behavior from a monoexponential decay ($K = 0$ when the diffusion-driven molecular displacements obey a Gaussian law), a marker of the heterogeneity of the diffusion environment.

Signal attenuation was also fitted using the biexponential model equation:

$$F_{\text{diff}} = f_{\text{slow}} \cdot \exp(-bD_{\text{slow}}) + (1 - f_{\text{slow}}) \cdot \exp(-bD_{\text{fast}}) , \quad (3)$$

where f_{fast} and f_{slow} and D_{fast} and D_{slow} are the relative fractions and diffusion coefficients of a fast and a slow pool, respectively. This biexponential function is known to capture the diffusion MRI signal attenuation pattern very well, up to large *b* values.[17,18]

To bridge these 2 models and make comparisons easier (not only within this study but also with other literature data), an average diffusion coefficient <*D*> (derivative of F_{diff} from Eq. 3 when *b* approaches 0) was estimated from the biexponential model, as the kurtosis ADCo equivalent:

$$\langle D \rangle = f_{\text{slow}} D_{\text{slow}} + (1 - f_{\text{slow}}) D_{\text{fast}} \text{ ADCo} . \quad (4)$$

Similarly, at second-order level, a biexponential index (BI) can be derived as a kurtosis equivalent from the parameters of the biexponential model, as

$$\text{BI} = 3\left[\left(f_{\text{slow}} D_{\text{slow}}^2 + (1 - f_{\text{slow}}) D_{\text{fast}}^2 \right) / \langle D \rangle^2 - 1 \right] \equiv K . \quad (5)$$

The biexponential index also quantifies the degree of non-monoexponentiality (BI = 0 when $D_{\text{slow}} = D_{\text{fast}}$).

Then, estimates of perfusion parameters, f_{IVIM} and F_{perf}, were obtained by fitting the residual of the measured signal for b less than 300 s/mm^2 after the diffusion component has been removed:

$$f_{IVIM}F_{perf} = S/So - (1 - f_{IVIM})F_{diff}\ , \quad (6)$$

using for F_{perf} a simple model[19]:

$$F_{perf} = \exp[\ -b.D^*]\ , \quad (7)$$

where D^* is the pseudo-diffusion coefficient associated to the IVIM effect (which also includes the diffusion coefficient of water in blood).

This 2-step process was performed on a voxel-by-voxel basis, providing parametric maps of diffusion and perfusion IVIM parameters, as well as on a region-of-interest basis, using the nonlinear subspace trust region fitting algorithm built into Matlab (MathWorks, Natick, MA). Regions of interest in the tumor were drawn manually using the reference anatomical images as a guidance to avoid necrotic parts. The diffusion and perfusion parameters were obtained from the contralateral side as a control. Region-of-interest analyses were performed on the tumor and the contralateral side, respectively.

Quantification of Microvessel Density and Tumor Cellularity

The expression of vWF in gliomas was counted as microvessel density (MVD).[20] Tumor cellularity was evaluated as described previously.[21] Low power light microscopy (magnification, ×40 and ×100) was used to scan the heterogeneous tumor sections for areas with high neovascularization. Any single positive-stained cell or cluster of endothelial cells that was clearly separate from adjacent microvessels, tumor cells, and other connective tissue elements was considered to be a vessel. For the quantification of MVD and tumor cellularity, 10 areas with the greatest vascular density or tumor cellularity were visually selected by 2 observers in consensus at low power field (×100) and then captured for each tumor at high power field (0.17 mm^2 at ×400 magnification) using a camera mounted on a Zeiss microscope (Carl Zeiss, Gottingen, Germany) and AxioVision Rel. 4.8.2 Software (Carl Zeiss, Thornwood, NY). Individual microvessel counts were conducted in all 10 areas, and nuclei of tumor cells were counted in 3 areas with the greatest tumor cellularity (visually selected out of the 10 areas). The presence of red blood cells or a vessel lumen was not required for a structure to be classified as a microvessel. The MVD or the tumor cellularity was expressed as the mean number of vessels or nuclei of tumor cells in these areas.

TABLE 1. Diffusion and Perfusion Parameters in Tumor and Contralateral Side Obtained With Kurtosis and Biexponenital Diffusion Model (Mean Values and 95% Confidence Interval)

Parameter	Tumor	Contralateral Side	*P*
ADCo, 10^{-3} mm^2/s	0.749 (0.684–0.814)	0.746 (0.686–0.807)	0.95
<*D*>, 10^{-3} mm^2/s	0.826 (0.772–0.880)	0.774 (0.703–0.846)	0.10
K	0.818 (0.764–0.872)	0.623 (0.562–0.685)	<0.0001
BI	0.898 (0.725–1.070)	0.529 (0.399–0.659)	<0.001
f_{slow}	0.436 (0.379–0.493)	0.368 (0.276–0.459)	<0.05
D_{fast}, 10^{-3} mm^2/s	1.27 (1.15–1.39)	1.10 (0.920–1.29)	<0.01
D_{slow}, 10^{-4} mm^2/s	2.78 (2.48–3.07)	2.90 (2.23–3.57)	0.57
f_{IVIM}, %†	2.75 (1.94–3.57)	0.84 (0.42–1.26)	<0.001
D^*, 10^{-2} mm^2/s†	0.545 (0.379–0.710)	1.62 (0.559–2.69)	0.06

Parameter estimates in the tumor were obtained from 14 rats (scanned either at day 7 or 12). Perfusion parameters for the contralateral side were estimated from 9 rats.

ADC indicates apparent diffusion coefficient; BI, biexponential index.

†Perfusion parameters were obtained after removing the diffusion component of the signal (kurtosis diffusion model).

TABLE 2. Diffusion and Perfusion Parameters in Tumor Obtained With Kurtosis and Biexponenital Diffusion Model at Days 7 and 12 (Mean Values and 95% Confidence Interval)

Parameter	Tumor at Day 7	Tumor at Day 12	*P*
ADCo, 10^{-3} mm^2/s	0.835 (0.796–0.874)	0.685 (0.595–0.774)	<0.01
<*D*>, 10^{-3} mm^2/s	0.913 (0.843–0.982)	0.761 (0.725–0.796)	<0.001
K	0.790 (0.744–0.837)	0.839 (0.742–0.936)	0.35
BI	0.862 (0.766–0.958)	0.924 (0.592–1.257)	0.71
f_{slow}	0.434 (0.404–0.464)	0.437 (0.327–0.548)	0.95
D_{fast}, 10^{-3} mm^2/s	1.38 (1.24–1.52)	1.19 (1.00–1.38)	0.09
D_{slow}, 10^{-4} mm^2/s	3.08 (2.68–3.47)	2.55 (2.15–2.95)	<0.05
f_{IVIM}, %†	3.41 (3.14–3.68)	1.25 (0.763–1.74)	<0.0001
D^*, 10^{-2} mm^2/s†	0.669 (0.632–0.706)	0.839 (−0.416–2.093)	0.79
Tumor cellularity (cells/field)	592.2 (558.8–625.6)	611.2 (564.7–657.7)	0.47
MVD (vessels/field)	42 (28.1–55.9)	25.5 (19.1–31.8)	0.01

†Perfusion parameters were obtained after removing the diffusion component of the signal (kurtosis diffusion model). ADC indicates apparent diffusion coefficient;

BI indicates biexponential index; MVD, microvessel density.

Statistical Analysis

All the parameters in the tumors and contralateral side were compared with paired-samples t test. Two-samples t test was used for comparison of parameters at 7 and 12 days after implantation. Correlation between diffusion/perfusion MRI and histopathological parameters was evaluated using Pearson correlation coefficient. For all tests, a P value <0.05 was considered statistically significant. All statistical analyses were conducted by using statistical software Medcalc (version 11.3.2.0, Mariakerke, Belgium).

RESULTS

The average diffusion and perfusion parameters obtained from all animals (images collected at days 7 and 12) within the tumors and the contralateral basal ganglia are summarized in Table 1. A comparison of the parameters obtained after 7 and 12 days after implantation is shown in Table 2 and Table 3. Examples of representative parametric maps are shown in Figures 1 and 2. The tumor diameter increased from 5.81 ± 0.64 mm at 7 days to 7.47 ± 0.32 mm at 12 days.

Intravoxel incoherent motion maps clearly highlighted the areas with high and low fraction perfusion within tumors that appeared generally heterogeneous, as confirmed by histology. Variations in ADCo and kurtosis within the tumors were also common, underlying the known histological heterogeneity frequently observed in gliomas.[1]

Overall, global results obtained from the kurtosis and biexponential models were similar: ADCo and <*D*> were surprisingly not significantly different between the tumor and contralateral side, whereas a significant increase in K and BI was observed in the tumor ($P < 0.0001$ and $P < 0.001$, respectively). However, the biexponential model revealed that both f_{slow} and D_{fast} increased ($P < 0.05$ and $P < 0.01$, respectively), in agreement with Hoff et al,[22] explaining the apparent stability in <*D*> toward which they have opposite effects. D_{slow} in the tumor and the contralateral side was not significantly different, but D_{slow} significantly decreased between days 7 and 12 ($P < 0.05$). Indeed, ADCo and <*D*> significantly decreased between days 7 and 12 in the tumor ($P < 0.01$ and $P < 0.001$, respectively), from values

TABLE 3. Diffusion Parameters in Contralateral Side (Kurtosis Model) at Days 7 and 12 (Mean Values and 95% Confidence Interval)

Parameter	Contralateral Side at Day 7	Contralateral Side at Day 12	*P*
ADCo, 10^{-3} mm^2/s	0.799 (0.767–0.832)	0.707 (0.603–0.810)	0.10
K	0.635 (0.537–0.732)	0.615 (0.513–0.717)	0.75

ADC indicates apparent diffusion coefficient.

slightly higher than for the contralateral side at day 7 to slightly lower values at day 12. This decrease pattern in <*D*> during tumor growth has been observed by other groups, and we found a negative correlation between <*D*> and tumor cell count (H&E) with a correlation coefficient of −0.70 ($P < 0.01$) (Fig. 3). There was a negative, but not significant, trend between ADCo and tumor cell count with a correlation of $r = -0.33$ ($P = 0.25$). On the other hand, *K* and BI were significantly higher in the tumor already at day 7, further increasing (but without statistical significance) at day 12, suggesting that those indices are more sensitive biomarkers of tumor growth than ADCo or <*D*> is.

Regarding perfusion, f_{IVIM} in the tumor was significantly higher than in contralateral basal ganglia ($P < 0.001$), as expected from neovascularization. Indeed, there was a significant positive correlation between f_{IVIM} and MVD, with a correlation coefficient of 0.56 ($P < 0.05$) (Fig. 4). f_{IVIM} at day 12 was significantly lower than at day 7 ($P < 0.0001$), in accordance with the decrease in the number of the tumor vessels on vWF ($P = 0.01$). *D** in the tumor was slightly lower than in contralateral basal ganglia (although the difference was not significant), perhaps reflecting a lower flow (less functional) pattern than in normal microvasculature.

DISCUSSION

The use of diffusion and IVIM MRI for diagnosis and monitoring of cancer is steadily increasing. In the brain, gliomas are the most common primary tumor, and the 9L rat brain glioma model has been the widely used as experimental preclinical model. Here, we have used this model to investigate the effect of tumor features, such as neovascularization and cell proliferation, on parameters that can be obtained from IVIM and diffusion MRI used as an imaging cancer biomarker. We found significant differences in those parameters estimated at 17.2 T between the tumors and the contralateral side, both for perfusion and non-Gaussian diffusion. Those differences were supported by histological findings. Each parameter map clearly highlighted the tumor heterogeneity, as supported by histological findings. The use of diffusion and perfusion parameters, as obtained with IVIM MRI, might be useful for biopsy guidance within gliomas, which are notoriously heterogeneous.[23]

Diffusion parameters, such as ADCo, <*D*>, *K*, and BI, provide information on tissue microstructure. *K* and BI, markers of non-Gaussian diffusion from the kurtosis and biexponential model, respectively, were found equivalent and were significantly higher in the tumors compared with the contralateral side, whereas ADCo and <*D*> were not. This finding suggests that the deviation from Gaussianity is a more sensitive index that average diffusion to characterize tumor growth, reflecting an increased interaction of water molecules with

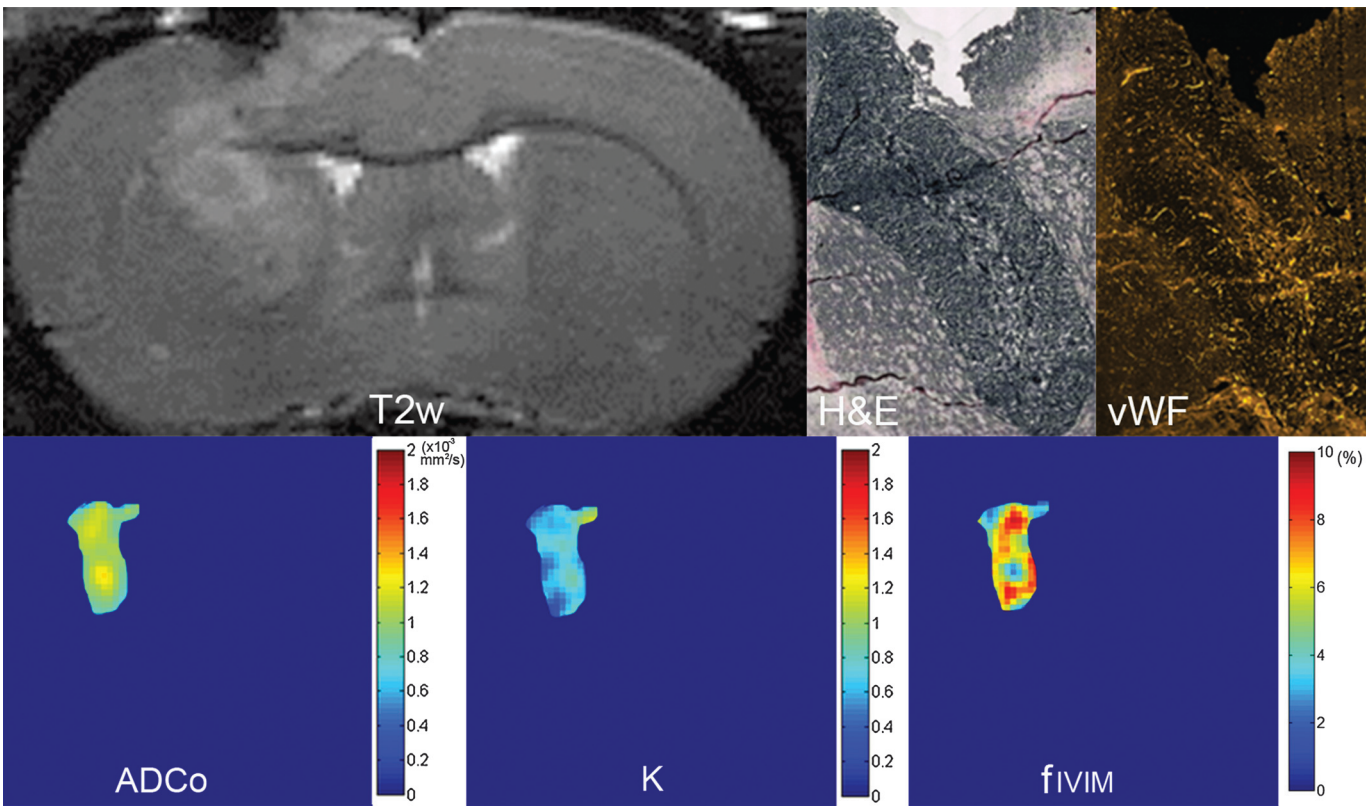

FIGURE 1. The tumor at day 7 is identified in the left basal ganglia on the T2w image. The tumor exhibits parts with a very high f_{IVIM} fraction and a central part with low f_{IVIM} fraction and high ADCo. On the ADCo and *K* maps, the tumor looks heterogeneous with high values in the upper part of the tumor where f_{IVIM} is also high. There are many tumor cells visible on the H&E image, especially at the periphery of the tumor, as well as many tumor vessels visible in the vWF immunohistological images.

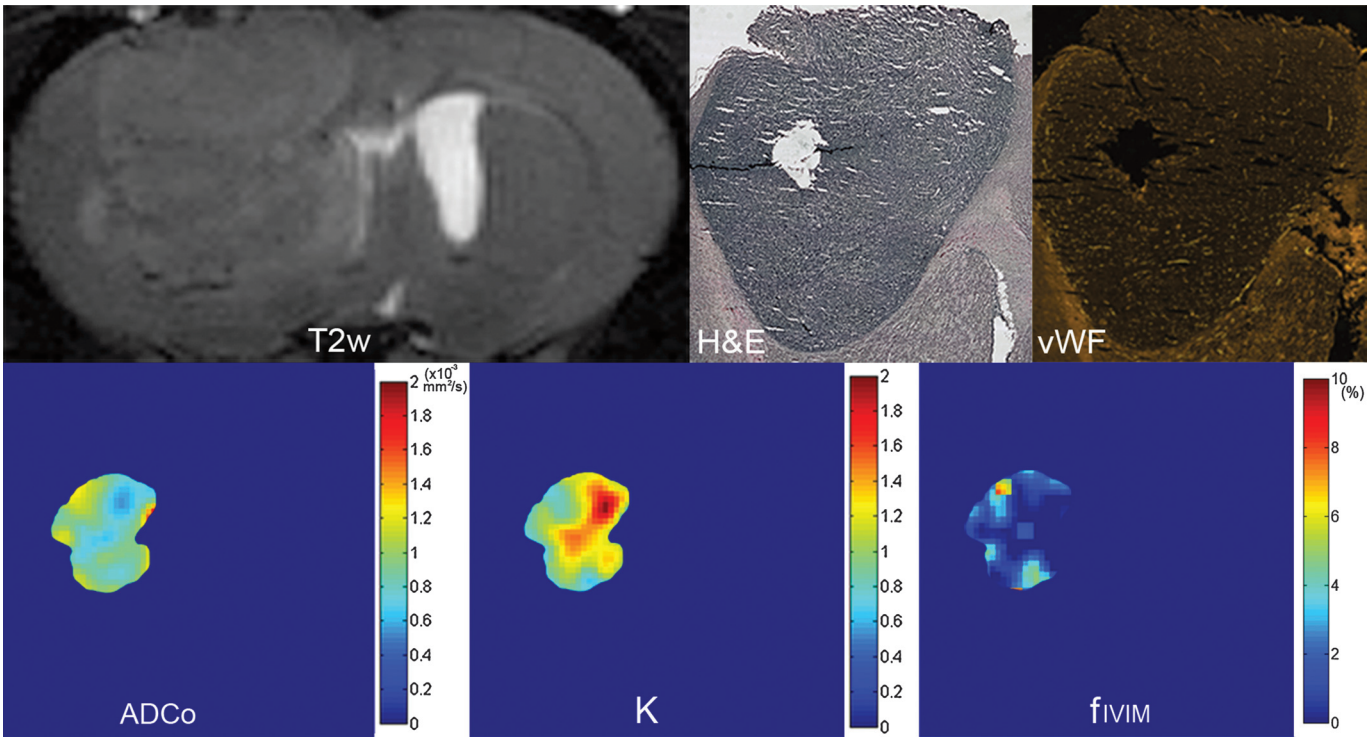

FIGURE 2. The tumor at day 12 occupies the entire left basal ganglia on the T2w image. f_{IVIM} is very low in contrast to that of the tumor in Figure 1. ADCo is also relatively low, but kurtosis appears very high in some parts of the tumor. The tumor vessels are relatively few on the vWF image, corresponding to low fraction on f_{IVIM} map. Cell distribution looks more homogeneous on the H&E image, compared with the tumor in Figure 1.

tumor cells (increase in membrane density from cell proliferation, but this mechanism remains to demonstrate). However, <*D*> was found to be inversely correlated with cell density, as observed by another group,[5] and decreased between days 7 and 12, a result also observed in a C6 rat glioma study.[21] Interestingly, D_{fast} from the biexponential model was found higher in the tumor, which could perhaps suggest less hindrance (tortuosity) effects in the extracellular space, despite cell proliferation. This result is consistent with those of Vonarbourg et al,[24] who showed a higher ADC ($0.85 \pm 0.02 \times 10^{-3}$ mm^2/s in tumor vs 0.59 ± 0.02 mm^2/s in contralateral side) in 9L glioma, suspecting central necrosis or edema. Another group showed an ADC increase at 1 week after implantation of C6 gliomas to rats.[21] Indeed, this tumor model has a sarcoma appearance with limited cell invasion in the periphery despite of the rapidness of the tumor growth, suggesting that the extracellular space or edema might be larger in 9L gliomas, as shown by T2 increase in 9L glioma.[24] However, glioma invasion to white matter is possible, often seen in a regular pattern,[25] but this point was not investigated in this study (only 1 diffusion direction was sampled, precluding accurate results in anisotropic white matter). Moreover, variability in cell size or nucleus to cell size ratio might also influence the diffusion findings between normal and tumor tissues. Variations in the linear cell dimension could also be interesting to investigate, as it could be better correlated with diffusion parameters.

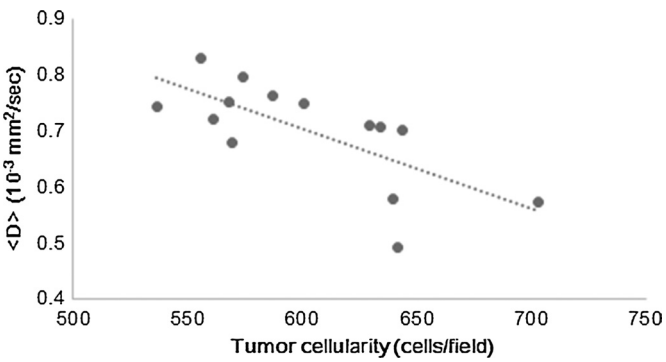

FIGURE 3. <*D*> versus tumor cell counts on H&E stained image (0.17 mm^2 at ×400 magnification). There was a negative correlation between tumor cell count and <*D*>, with a correlation coefficient of −0.70 ($P < 0.01$).

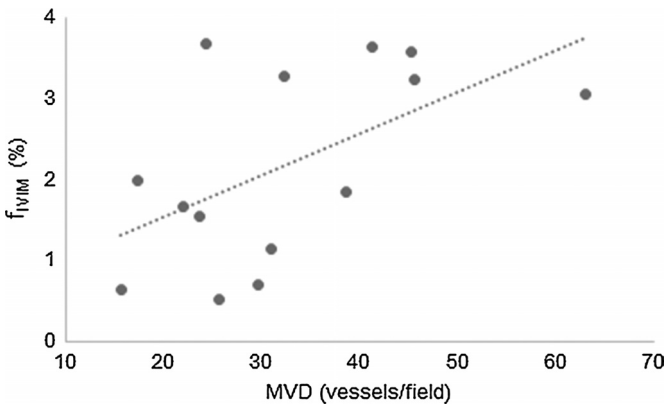

FIGURE 4. f_{IVIM} from kurtosis model versus microvascular density counts on vWF stained image (0.17 mm^2 at ×400 magnification). A positive correlation between f_{IVIM} and MVD was found, with a correlation coefficient of 0.56 ($P < 0.05$).

D_{slow} estimated from the biexponential model, however, showed no significant difference between the tumor and contralateral side but decreased with tumor growth. f_{slow}, the fraction of the slow water pool, was higher in the tumor, which is partially responsible for the increase noted in K and BI, perhaps reflecting an increased interaction of water with cell membranes, the surface of which increases with cell proliferation. Although this interpretation remains speculative at this stage, it underlines not only the potential of diffusion MRI to characterize tumoral tissue but also the need to develop more sophisticated, explanatory models of water diffusion behavior in tissues.

Parameters of the kurtosis and the biexponential model can be mathematically linked together, facilitating comparisons between the models and also with literature. Diffusion parameters from the biexponential model were found, however, to be very sensitive to noise and the initial values used for data fitting. Parameters from the kurtosis model, which has 1 less degree of freedom, were a little more robust. However, the kurtosis model is known to lose accuracy when using b values greater than 2000 to 2500 s/mm^2, whereas the biexponential model has been shown to work with much higher b values. Hence, although $<D>$ and BI are mathematically equivalent to ADCo and K, respectively, differences can be found because of those known limitations. Furthermore, the biexponential model, as shown in this study, can provide additional valuable information on diffusion through f_{slow}, D_{fast}, or D_{slow}.

Another interesting feature of IVIM MRI is that perfusion-related parameters can be obtained using the same data sets without the need for contrast agents. There was an increase in f_{IVIM} in the tumors and a positive correlation between f_{IVIM} and tumor vessel counts (vessel count per volume might have correlated even better but was not available for this study), suggesting that IVIM reflects the microvasular blood volume. Federau et al[12] found a moderate correlation between f_{IVIM} (obtained from a monoexponential diffusion model) and dynamic susceptibility contrast-based cerebral blood volume (CBV) in human brain glioma. However, dynamic susceptibility contrast-based CBV is sensitive to vessel wall permeability, whereas f_{IVIM} reflects only blood flowing in small vessels. Interestingly, f_{IVIM} significantly decreased at day 12 compared with day 7 after implantation. This result is consistent with the decrease in CBV observed between 3 and 4 weeks in a mouse glioma model.[26] One should be aware, however, that f_{IVIM} represents the T1w, T2w volume fraction of incoherently flowing blood. Relaxation effects must be removed to retrieve the actual flowing blood volume. Taking literature values for blood relaxivity at 3 T,[27,28] flowing blood volume values would be approximately 2.2 times the f_{IVIM} values. On the other hand, D*, which is related to the blood flow,[29] was slightly (with no significant difference) lower in the tumor, perhaps suggesting the poorly functional nature of neovessels. However, the standard deviation in our estimated D* was very high, and this parameter proved difficult to estimate with good accuracy. In human glioma, perfusion parameters showed significant difference between high- and low-grade glioma,[12] including D*. Indeed, further studies using DCE-MRI to measure values of tissue blood flow within the tumors need to be performed. Furthermore, the theoretical relationship between IVIM parameters and tissue perfusion has been established long ago,[29] and more modeling would be welcome, an important step to better understand which vessels contribute to the IVIM effects and to optimize the imaging acquisition protocols used clinically.

CONCLUSION

In conclusion, IVIM MRI appears as a very promising approach providing information on microcirculation and tissue microstructure to improve characterization of brain tumors, as confirmed from histology. With IVIM MRI, perfusion-related parameters can be derived without the need for contrast agents. Information on tissue microstructure can be obtained by looking at the non-Gaussian diffusion behavior of water, using models such as the kurtosis or the biexpoential diffusion model.

REFERENCES

1. Johnson P, Hunt S, Drayer B. Human cerebral gliomas: correlation of postmortem MR imaging and neuropathologic findings. *Radiology.* 1989;170:211–217.
2. Le Bihan D, Turner R, Douek P, et al. Diffusion MR imaging: clinical applications. *AJR Am J Roentgenol*. 1992;159:591–599.
3. Yamasaki F, Kurisu K, Satoh K, et al. Apparent diffusion coefficient of human brain tumors at MR imaging. *Radiology.* 2005;235:985–991.
4. Koh DM, Collins DJ. Diffusion-weighted MRI in the body: applications and challenges in oncology. *AJR Am J Roentgenol*. 2007;188:1622–1635.
5. Chenevert TL, Stegman LD, Taylor JMG, et al. Diffusion magnetic resonance imaging: an early surrogate marker of therapeutic efficacy in brain tumors. *J Natl Cancer Inst*. 2000;92:2029–2036.
6. Le Bihan D. The 'wet mind': water and functional neuroimaging. *Phys Med Biol*. 2007;52:57–90.
7. Le Bihan D. Apparent diffusion coefficient and beyond: what diffusion MR imaging can tell us about tissue structure. *Radiology.* 2013;268:318–322.
8. Le Bihan D. Intravoxel incoherent motion imaging using steady-state free precession. *Magn Reson Med*. 1988;7:346–351.
9. Le Bihan D, Breton E, Lallemand D. Perfusion in intravoxel incoherent motion MR imaging. *Radiology.* 1988;168:497–505.
10. Le Bihan D. Intravoxel incoherent motion perfusion MR imaging: a wake-up call. *Radiology.* 2008;249:748–752.
11. Koh DM, Collins DJ, Orton MR. Intravoxel incoherent motion in body diffusion-weighted MRI: reality and challenges. *AJR Am J Roentgenol*. 2011; 196:1351–1361.
12. Federau C, Meuli R, O'Brien K, et al. Perfusion measurement in brain gliomas with intravoxel incoherent motion MRI [published online ahead of print August 22, 2013]. *Am J Neuroradiol*.
13. Kim HS, Suh CH, Kim N, et al. Histogram analysis of intravoxel incoherent motion for differentiating recurrent tumor from treatment effect in patients with glioblastoma: initial clinical experience [published online ahead of print August 22, 2013]. *Am J Neuroradiol*.
14. Goldbrunner RH, Wagner S, Roosen K, et al. Models for assessment of angiogenesis in gliomas. *J Neuro-oncol*. 2000;50:53–62.
15. Prince MR, Zhang HL, Roditi GH, et al. Risk factors for NSF: a literature review. *J Magn Reson Imaging*. 2009;30:1298–1308.
16. Jensen JH, Helpern JA. MRI quantification of non-Gaussian water diffusion by kurtosis analysis. *NMR Biomed*. 2010;23:698–710.
17. Niendorf T, Dijkhuizen RM, Norris DG, et al. Biexponential diffusion attenuation in various states of brain tissue: implications for diffusion-weighted imaging. *Magn Reson Med*. 1996;36:847–857.
18. Pyatigorskaya N, Le Bihan D, Reynaud O, et al. Relationship between the diffusion time and the diffusion MRI signal observed at 17.2 tesla in the healthy rat brain cortex [published online ahead of print September 10, 2013]. *Magn Reson Med.*
19. Le Bihan D, Breton E, Lallemand D, et al. Separation of diffusion and perfusion in intravoxel incoherent motion MR imaging. *Radiology.* 1988;168:497–505.
20. Weidner N. Current pathologic methods for measuring intratumoral microvessel density within breast carcinoma and other solid tumors. *Breast Cancer Res Treat*. 1995;36:169–180.
21. Fan G, Zang P, Jing F, et al. Usefulness of diffusion/perfusion-weighted MRI in rat gliomas: correlation with histopathology. *Acad Radiol*. 2005;12:640–651.
22. Hoff BA, Chenevert TL, Bhojani MS, et al. Assessment of multiexponential diffusion features as MRI cancer therapy response metrics. *Magn Reson Med*. 2010;64:1499–1509.
23. Weber M-A, Henze M, Tüttenberg J, et al. Biopsy targeting gliomas: do functional imaging techniques identify similar target areas? *Invest Radiol*. 2010;45:755–768.
24. Vonarbourg A, Sapin A, Lemaire L, et al. Characterization and detection of experimental rat gliomas using magnetic resonance imaging. *Magn Reson Mater Phys Biol Med*. 2004;17:133–139.
25. Zhang J, van Zijl P, Laterra J, et al. Unique patterns of diffusion directionality in rat brain tumors revealed by high-resolution diffusion tensor MRI. *Magn Reson Med*. 2007;58:454–462.
26. Cha S, Johnson G, Wadghiri YZ, et al. Dynamic, contrast-enhanced perfusion MRI in mouse gliomas: correlation with histopathology. *Magn Reson Med*. 2003;49:848–855.
27. Lu H, Clingman C, Golay X, et al. Determining the longitudinal relaxation time (T1) of blood at 3.0 Tesla. *Magn Reson Med*. 2004;52:679–682.
28. Uludağ K, Müller-Bierl B, Uğurbil K. An integrative model for neuronal activity-induced signal changes for gradient and spin echo functional imaging. *Neuroimage*. 2009;48:150–165.
29. Le Bihan D, Turner R. The capillary network: a link between IVIM and classical perfusion. *Magn Reson Med*. 1992;27:171–178.